Unravelling Antarctica's past through the stratigraphy of a deep ice core: an image-analysis study of the EPICA-DML line-scan images

Gonzalo Morcillo Juliani(1); Sérgio Henrique Faria(1,2); Sepp Kipfstuhl(3,4)

(1) Basque Centre for Climate Change (BC3), 48940 Leioa, Spain

(2) IKERBASQUE, Basque Foundation for Science, 48011 Bilbao, Spain

(3) Alfred Wegener Institute, Helmholtz Centre for Polar and Marine Research (AWI), 27568 Bremerhaven, Germany

(4) Physics of Ice, Climate, and Earth, Niels Bohr Institute, University of Copenhagen, Denmark

Abstract:

Polar ice research has undergone great progress in the last six decades. One of its recent technological achievements has been the development of new techniques for digital image recording and analysis of ice-core stratigraphy and microstructure. In this work we investigate one such image records, namely the line-scan image records of the EPICA-DML (European Project for Ice Coring in Antarctica, Dronning Maud Land) deep ice core. These images provide a multiscale depiction of the stratigraphy and structure of the Antarctic Ice Sheet. While previous studies have focused on the ice-core optical stratigraphy on the micro- and mesoscale (< 1 mm and 10^{-3}–1 m, respectively), in this work we present several methods to obtain fast and reliable information on the ice-core stratigraphy on the macroscale (1–10^{3} m), including the full ice-sheet thickness. The paleoclimatic relevance of the ice-core optical stratigraphy on the macroscale is demonstrated through the comparison of the line-scan grey-value record of the EPICA-DML deep ice core with its mineral dust record, which is used as a proxy for microinclusions and for several other types of climate proxies. Additionally, we introduce a novel method to estimate the macroscopic air-bubble concentration (including number and size of bubbles) in ice cores, which is simpler, faster, and almost as reliable as painstaking microscopic studies. After a brief excursion on the relation between macroscopic and mesoscopic measures of optical stratigraphy, we close this work by making the case for a multi-measure analysis of ice-core line-scan images, which enables us to obtain a broad perspective of the optical stratigraphy of the whole ice core, with relevance for paleoclimate and ice-sheet-flow studies.

Key words: Antarctica, image analysis, ice cores, EDML

1. INTRODUCTION

One of the greatest achievements of polar research has been the ice core drilling to bedrock through the deep ice sheets on both hemispheres (e.g. NorthGRIP, GISP2, Dome C, Dome Fuji, etc.; see Faria et al., 2014a, for a recent review). Scientific results derived from the analysis of these ice cores have led to great progress in glaciology, meteorology, and for the understanding of Earth's climate system (e.g. NorthGRIP Members, 2004; Gow et al., 1997; EPICA Community Members, 2004, 2006; Kawamura et al., 2007).

The deep ice core retrieved in one of those drilling programs, namely the EPICA-DML (European Project for Ice Coring in Antarctica, Dronning Maud Land), was extracted from the Atlantic sector of Antarctica (Oerter et al., 2009). It has been stored and scanned with a special ice-core line-scanner in the cold facilities of the Alfred Wegener Institute (AWI) in Bremerhaven, Germany (Lambrecht et al., 2004). A collection of the pre-processed line-scan images, covering the whole EPICA-DML deep ice core from 450 m depth down to the bed at 2774 m depth, was later published by Faria et al. (2018). It is this latter collection of high-quality, greyscale, line-scan digital images, here called EDML-LS images, which is the object of this study. They display in great detail the optical stratigraphy of the EPICA-DML deep ice core, which is illustrated and summarized in Fig. 1.

The fundamentals of grey-value analysis of line-scan images have already been established in previous studies on the mesoscale (10^{-3}–1 m) mainly involving the NorthGRIP deep ice core (Svensson et al., 2005, Winstrup et al., 2012), the Dome Fuji deep ice core (Takata et al., 2004), and the WAIS drilling project (McGwire et al., 2008). One of the main features of these studies is the identification of cloudy bands (Gow and Williamson, 1976), which appear in ice cores as characteristic opaque strata. Their opacity is normally related to a high concentration of microscopic inclusions, called microinclusions, in particular mineral dust and salt particles (Faria et al., 2010). Thus, number and size of cloudy bands in ice core samples are ultimately related to climate events, involving changes in precipitation, temperature, and atmospheric transport of aerosols.

The relation between different impurities found in polar ice and the optical stratigraphy have been investigated by Takata et al. (2004), Svensson et al. (2005) and Winstrup et al. (2012). Both, Takata et al. (2004) and Svensson et al. (2005) offer pioneering overviews of the relation between mesoscopic optical stratigraphy and ice-core paleoclimate records. They present a comprehensive list of physical and chemical properties of deep polar ice that influence the optical stratigraphy, as well as a method for locating and interpreting annual accumulation layers. The same research path was followed by McGwire et al. (2008) and Winstrup et al. (2012), with the latter presenting the first steps towards a mathematical approach, based on hidden Markov modelling, for an automated method of annual layer counting. These works established the foundations of the optical stratigraphy analysis of ice cores via line-scan images.

The relation between the concentration of air bubbles and cloudy bands has been studied in microscopic (< 1 mm) detail via Microstructure Mapping by Ueltzhöffer et al. (2010) and Bendel et al. (2013). Starting from the known observations that cloudy-band ice is generally fine-grained and rich in microinclusions, these studies demonstrated that cloudy bands also have smaller air bubbles in larger number than the neighbouring clear-ice strata. A mesoscopic (10^{-3}–1 m) or macroscopic (> 1 m) counterpart of these studies has been difficult, however, because the intense light scattering by air bubbles makes it hard to distinguish optical stratigraphic features.

In this work we present a macroscopic, multi-measure analysis of ice-core line-scan images, which combines the conventional stratigraphic description through grey values with a novel proxy for the concentration of air bubbles (including number and size) via binarized bright-spot analysis. In Section 2 we present the methodological foundations of the analysis. A multiscale description of the EPICA-DML optical stratigraphy is given in Section 3, together with a combined analysis of grey values, binarized bright spots, minimum and maximum pixel values. At last, conclusions and recommendations for future measurements and analyses are discussed in Section 4.

2. METHODS

The EPICA-DML (also called EDML) deep ice core was drilled next to Kohnen Station (75°00’09’’S, 00°04’06’’E, 2892 m a.s.l.) and has reached a depth of 2774.15 m. It was transported from Antarctica to Europe during two months at -25 °C and was subsequently stored at -28 °C in the cold facilities of the Alfred Wegener Institute (AWI) in Bremerhaven, Germany, for an additional period of 3–4 months. Ice-core slabs with dimensions close to 1000 × 98 × 33 mm (length × width × thickness) were prepared and scanned with an automatic line-scan device within 2 days at -20 °C. The preparation of the samples included cutting the slabs with a band saw and polishing both surfaces perpendicular to the thickness by hand with a microtome knife. To minimize the effects of surface imperfections and variations in sample thickness, the camera and the oblique light beams were focused on a focal plane within the ice slab. As the core was scanned immediately after cutting, pressure-induced formation of new or strange bubble features was very limited. The resulting high-resolution photographs produced with the EDML line-scanner, here called EDML LS images, have circa 9 cm of width and 110 cm of length (Faria et al., 2018).

To obtain accurate measurements during image analysis, we first processed the LS images by adjusting and repairing artefacts and technical defects. For that purpose, we employed methods similar to those used by Winstrup (2011), as described below.

2.1. Line-scan device

The EPICA-DML line-scanner is a device capable of scanning axial-wise prepared ice-core slabs. It is equipped with an oblique illumination system on dark field, which enhances the contrast of impurities and inclusions in the ice core. When inclusions in the ice slab are illuminated by the light beam, they reflect and refract the light, scattering it in all directions (Fig. 2). Part of the scattered light is captured by the lens of the camera, reaching the CCD (charged coupled device) sensor, where the image is recorded. The linear resolution of the EPICA-DML line-scanner is 115 pixels per centimetre.

2.2. Image processing

Features of the raw images recorded with the line-scan device are slightly affected by various extrinsic factors, including scratches and notches on the sample surfaces, ambient lighting, operator's adjustments, wear of the device, and other factors. Therefore, the LS images need some fine adjustments before being combined to generate a continuous stratigraphic profile. We have digitally processed the LS images using the *ImageJ* software (Schneider et al., 2012) and employed a sequence of image adjustments similar to those described by Winstrup (2011). This includes contrast adjustment, longitudinal grey-value-trend alignment, and the removal of spurious white spots and other sample-surface imperfections from the images. Finally, depending on the case, we matched the grey values at the boundaries of neighbouring images either with the help of the Wilcoxon signed-rank test (Rey and Neuhäuser, 2011), or matching the least squares adjustment lines, with a confidence interval based on the mean and the standard deviation.

2.3. Grey value measures

Grey value, defined as the relative degree of lightness or darkness of a pixel, is the main and most fundamental parameter in greyscale image analysis. In 8-bit images, grey values may range from 0 (black) to 255 (white), thus covering 256 possible pixel values. In theory, the grey value of any pixel in the line-scanned image of an ideally pure and homogeneous piece of ice should be zero. In practice, however, the zero value is rarely reached by any pixel.

Grey-value analysis can be performed over an entire image, or in a selected region of it, with a diversity of statistical measures, including the mode, the median, and various types of means of the grey-value distribution, the minimum and maximum pixel value in the region, etc. As in previous studies of LS images, here we adopt the mean grey value as the conventional measure of optical stratigraphy throughout the ice core.

What is precisely meant by "mean" deserves a brief clarification here, since this term is generally used to refer not only to any of the various types of statistical mean, but also in a loose sense to other measures of central tendency, like the median or the mode. We have tested various measures of grey value, including the geometric mean, median, minimum and maximum pixel value. On the macroscale, we found that these measures yield essentially similar information for 8-bit LS images, with the arithmetic mean performing best, because of its higher sensitivity to bright spots, which are most relevant for LS images. The median suffers from the fact that it can assume only integer values in 8-bit images, which limits the definition of grey values in darker images (clear ice). The minimum and maximum pixel values are particularly useful on the mesoscale, as described in Sect. 3.3. Owing to these results, here we define the *mean grey value* as the arithmetic mean of the density distribution of grey values within a selected region of the image.

For the macroscopic analyses described in this work, the selected region was always the same for all EDML LS images, as illustrated in Fig. 3. The region is a relatively narrow strip of circa 3 × 93 cm (350 × 10700 pixels). For simplicity, the selected region is roughly centred on the longitudinal axis of the image (not the core slab, which can show slight variations in position from one image to another). The ends of the core slab are excluded from the analysis (approx. 3 cm from each slab end), because of illumination artifacts from the top and bottom walls. On the macroscopic scale, such exclusions do not have any relevant effect. For higher-resolution analyses, such exclusions represent a loss of circa 5–6 % of each core slab, but that is tolerable and could hardly be recovered by any means.

Core breaks do not significantly influence the macroscopic analysis either, because they consist of two well-differentiated parts: a sharp peak that rises above the other grey values in the sample, and an equally sharp depression. The two effects practically cancel each other, with a net effect on the mean grey value that is not greater than 2 % or 5 %.

2.4. Bubble analysis

Meteoric ice is not simply frozen water. It is formed by sintering of snow crystals of precipitation (Faria et al., 2009, 2010). In this process, a little volume of air gets caught in the ice matrix, which by increasing pression turns into air bubbles. Thus, the most visible inclusions in meteoric ice are air bubbles. When a light beam hits a bubble, it must pass successively through two different media with contrasting refractive indices, namely ice and air. Therefore, the light beam will be diffracted according to Snell's Law and will reproduce the bubble contour (Hecht, 2016; Ueltzhöffer et al., 2010). On the other hand, the aerosol particles, which have much smaller sizes, will disperse the light according to the Mie dispersion model (Mie, 1908; Zúñiga and Crespo, 2010).

Statistical digital analysis of individual air bubbles is a powerful technique, as demonstrated by the painstaking microscopic investigations by Ueltzhöffer et al. (2010) and Bendel et al. (2013). In this work, we show for the first time that it is possible to obtain useful and interesting results also on the meso- and macroscale, through the definition of a suitable measure of bright spots described below.

The first and most fundamental step in any bubble analysis is to transform the greyscale image into a binary one. Image binarization is the process of classification of pixel values in two groups: white as foreground and black as background (Fig. 4). Therefore, binarization needs to be defined through a thresholding criterion. For this study we used ImageJ’s default threshold algorithm (a variation of the IsoData/Iterative Intermeans; see Ridler and Calvard, 1978), based on contrast, with a window of 15-pixel radius for the local mean.

In line-scan images, air bubbles appear as bright spots over a dark background. Since the linear resolution of the LS system is 115 pixels per centimetre, it follows that the minimum bubble size that can be resolved upon binarization of the EDML-LS images is ≈ 87 μm, which is the pixel size. For comparison, the precise microscopic analyses by Ueltzhöffer et al. (2010) and Bendel et al. (2013) have determined an average bubble diameter in the EPICA-DML ice core that gradually decreases with depth from circa 240 μm at 200 m to circa 140 μm at 1000 m depth (further down the bubbles gradually disappear through their transformation into clathrate hydrates; see Bendel et al., 2013; Faria et al., 2018 and references therein).

2.5. Mineral dust data

In contrast to ice cores from Greenland and elsewhere, a common feature of Antarctic ice cores is that several climate proxies vary more or less synchronously, including mineral dust, marine salts, and stable oxygen isotopes (EPICA Community Members, 2004, 2006; Fischer et al., 2007; Dome Fuji Ice Core Project Members, 2017; Wolff et al., 2006). This has the advantage that a multi-proxy comparison is not needed to determine the correlation of the optical stratigraphy with climate proxies (i.e., correlation with one proxy implies correlation with others), but it has the disadvantage that it is not possible to pinpoint the impurities that actually cause the optical stratigraphy.

Since mineral dust is one of the most stable and visible impurities in polar ice, it has been one of the major suspects of the formation of cloudy bands and optical stratigraphy (Gow and Williamson, 1976; Kipfstuhl et al., 2006, Faria et al., 2010, 2014b). Therefore, we selected it as the reference climate proxy for this study. As a side note, it should be remarked that cloudy bands are not made exclusively of mineral (terrestrial) dust: other substances, in particular sea salts, are often found in microinclusions (Eichler et al., 2019; Iizuka et al., 2009; Ohno et al., 2005; Oyabu et al. 2020; Sakurai et al. 2010). According to the recent study by Oyabu et al. (2020), the fractions of terrestrial dust, sea salt, and mixed (dust + sea salt) microinclusions found in the Antarctic ice cores are respectively 59 %, 11 %, and 27 % in the Dome Fuji deep ice core, and 47 %, 20 %, and 28 % in the EPICA-Dome C deep ice core.

Terrestrial mineral dust, mainly originated from arid and semiarid regions, is rich in carbonate particles, including calcite [$CaCO_3$] and dolomite [$CaMg(CO_3)_2$]. Since calcium has been routinely measured at high resolution in ice cores, it has often been used as a proxy for mineral dust, after correction for its sea-salt contribution. The corrected quantity, called non-sea salt calcium ($nssCa^{2+}$), was measured as a proxy for mineral dust in the EPICA-DML deep ice core by Fischer et al. (2007), using ion chromatography (IC). Here, we compare that mineral-dust proxy record with the data extracted from the optical stratigraphic analysis.

3. RESULTS AND DISCUSSION

3.1. Mean grey value and mineral dust

The dust depth-profile shows that mineral dust occurs in varying concentrations, related to distinct climatic events and periods (Wegner et al., 2012). In Fig. 5 we present the one-metre averaged depth profiles of mineral dust (Fischer et al., 2007) and mean grey value (EDML-LS images, this work) for the whole depth range of the EPICA-DML deep ice core where these data coexist (viz. 450–2416 m). Using the Antarctic ice core chronology (AICC2012) of Veres et al. (2012), we conclude that each one-metre depth-step corresponds to a variable period of time ranging from 20 years in the shallow depths to centuries in deep ice.

One of the first features that we can identify in the grey-value depth-profile in Fig. 5 is a marked dimorphism between shallow (bubbly ice) and deep (bubble-free ice) depths. The shallow portion on the left of the grey-value profile is characterized by a convex shape, while the central and deep parts on the right of the profile appear marked by a succession of peaks and valleys. Such a dimorphism complicates the grey-value analysis, since the methods used to analyse bubble-free ice are not suitable for analysing bubbly ice. To overcome this problem, we have used multiple measures that can be extracted from the line-scan images, in particular mean grey value and bright-spot concentration (Sects. 3.1 and 3.2), as well as minimum and maximum pixel values (Sect. 3.3).

From Fig. 5 we immediately observe that the macroscopic grey-value and dust profiles in the bubble-free ice zone (below 1200 m depth) seem to correlate quite well. Spectral analysis of these profiles in the depth range 1200–2416 m (Fig. 6) confirms that the relevant frequency peaks of both spectra (i.e., those peaks with power above the red-noise limit) do correlate very well, indeed. In fact, even the spectra below the red-noise limit show good correlation. This is a new and important result, which demonstrates that the optical stratigraphy of bubble-free ice does record the past climate quite reliably on the macroscale (1–10^3 m). In the range of frequencies above the red-noise limit, we can identify just one minor mismatch around 8 km^{-1} (which is nevertheless below the 80 % chi-squared bound), possibly caused by the mismatch of the profiles in the depth range 1200–1325 m, which marks the beginning of the bubble-free ice zone. The cause of this minor mismatch requires further investigation into the mesoscale (10^{-3}–1 m), and possibly the microscale (< 1 mm), which is evidently beyond the scope of this work (a first glimpse into de mesoscale is provided in Sect. 3.3).

3.2. *Bubbly ice and mineral dust*

Turning attention to the upper part of the core, it is evident that grey values are notably high in the depth range 450–1200 m, which corresponds to the bubbly-ice zone (Faria et al., 2018). Such high grey values are caused by the intense light scattering by air bubbles, which turns the line-scan images very bright, therefore masking dust-related stratigraphic features, like cloudy bands. The decay in grey values from 450 m to 800 m is related to a quasi-linear decrease in the mean bubble size with depth, driven by the increasing overburden pressure (Uelzhöffer et al., 2010). From 800 m to 1200 m grey levels decay even more dramatically, because of the gradual transformation of bubbles into air hydrates (which have a refraction index close to ice) within the bubble–hydrate transition zone (BHT; Faria et al., 2010, 2018).

Before starting the stratigraphic analysis of the bubbly-ice zone, we must recall some important results from recent microscopic investigations using the Microstructure Mapping method (Kipfstuhl et al., 2006; Faria et al., 2010, 2018; Bendel et al., 2013; Ueltzhöffer et al., 2010). These studies found correlations between the concentration of bubbles (considering both, size and number), the mean grain size of ice, and the concentration of mineral dust. Inspired by those results, we decided to test whether such a correlation is also detectable on the macroscale. To this aim, we performed the bubble analysis described in Sect. 2.4 (binarized bright-spot analysis). Our objective was to test the hypothesis that the number of bright spots observed in the LS images of bubbly ice (which are produced by the light scattering of air bubbles), could be used as a proxy for bubble concentration. The results of this analysis are shown in Figs. 7 and 8, which compare our proxy for bubble concentration with mineral dust data and the detailed microscopic analysis of air bubbles performed by Bendel et al. (2013).

As can be seen in Fig. 7, the macroscale correlation between the "real", microscopic bubble counting by Bendel et al. (2013) and our macroscopic counting of binarized bright spots is very good. Our proxy for the bubble number density successfully reproduces the correlation of dust concentration with the real bubble number density previously reported by Ueltzhöffer et al., (2010) and Bendel et al. (2013) (viz. a compound correlation: higher dust concentration–finer-grained ice–more and smaller bubbles), as well as the rate of bubble disappearance through their conversion into hydrates in the bubble–hydrate transition zone (BHT, 800–1200 m, Faria et al. 2010, 2018).

Likewise, Fig. 8 shows that the macroscale correlation between the "real" average bubble size derived from the microscopic analysis by Bendel et al. (2013) correlates very well with our macroscopic estimates of binarized bright-spot sizes. Our macroscopic proxy reproduces well the rate of decrease of the average bubble size with depth, driven by the increasing overburden pressure (Ueltzhöffer et al., 2010).

The novel results from Figs. 7 and 8 highlight the usefulness of the proposed binarized bright-spot analysis for studying the average number and size of air bubbles in ice cores on the macroscale, without the need to embark upon laborious and time-consuming microscopic analyses.

3.3. A brief excursion into the mesoscale

Sections 3.1 and 3.2 focused on macroscale features representing time intervals from many decades to millennia. As we move into smaller scales (from metres to millimetres), we start to see records of events in the range from decades to seasons. Previous studies (Svensson et al., 2005; Takata et al., 2004; Winstrup et al., 2012) have investigated a few individual samples on such a mesoscopic scale and could successfully identify optical stratigraphic signals of seasonal and annual cycles.

A detailed study of the EPICA-DML optical stratigraphy on the mesoscale is beyond the scope of this work. In this section we simply offer a glimpse into the mesoscale potential of the measures just proposed for LS image analysis. Our objective is not only to pave the way for future mesoscopic studies of line-scan images, but also to get a deeper multiscale understanding of the observations already described on the macroscale.

In Fig. 9 we see the mesoscopic details of two distinct EDML LS images, one from the bubbly-ice zone, and another one from the bubble-free-ice zone, together with superposed profiles of diverse measures. For better visualization, both images have been rotated 90° anti-clockwise, so that the strata appear as vertical bands and top is to the left.

The left panel (Fig. 9a) shows the mesoscopic details of a bubbly-ice sample from 449.45–449.60 m depth. The bright spots (bubble proxies) are evident and mask the microinclusion-rich cloudy bands. This is one of the clearest examples of optical stratigraphy in the bubbly-ice zone (450–1200 m) and still, even after the improvements of image processing, cloudy bands are hardly discernible. Plotted over the image are three profiles: mean grey value (blue, top), binarized bright-spot counting (yellow, middle) and minimum pixel value (red, bottom). In this case, the resolution of each graph is one millimetre, that is, each point in the graphs represents the average value of the respective measure calculated over a one-millimetre wide vertical stripe of the underlying image (i.e. parallel to the stratigraphy). The reason for choosing this one-millimetre resolution is because the bright-spot counting needs a stripe of reasonable width to encompass a few whole bubbles (bright spots).

The right panel (Fig. 9b) displays a typical example of the mesoscopic details of a sample from 1366.20–1366.25 m depth, within the central part of the bubble-free-ice zone of the EPICA-DML deep ice core. The glittering spots are mainly caused by specular reflections of the line-scanner light beam by the facets of polyhedral air hydrates. Several cloudy bands are clearly discernible. The superposed profiles are maximum pixel value (light grey, top), mean grey value (blue, middle), and minimum pixel value (red, bottom). These three profiles have been produced in the maximum resolution of one pixel (86.96 μm), that is, each point in the graphs represents the average value of the respective measure calculated over a one-pixel line running from top to bottom of the underlying image (i.e. parallel to the stratigraphy).

It is interesting to see how these distinct measures yield very similar profiles in both cases (bubbly and bubble-free ice), while revealing also distinct details of the stratigraphy. In both cases, the mean grey-value (blue) provides the clearest measure of the optical stratigraphy, capturing with precision all the main strata, because it is sensitive to a combination of all light scatters, including bubbles and microinclusions. The exclusive contribution of air bubbles to the light scattering of bubbly ice is distilled by the bubble-counting proxy (binarized bright-spot counting, in yellow). The similarity between the mean grey value and the binarized bright-spot counting is revealed by their Pearson cross-correlation coefficient, which has a value of 0.9. In bubble-free ice, the maximum pixel value (light grey) is particularly useful for detecting extra-fine layers lacking air hydrates, which are the sources of the most brilliant spots, in the absence of bubbles. Finally, the minimum pixel value shows a distinctively behaviour in each case. At first sight, it seems that the minimum pixel value just reproduces the results of the mean grey value. A careful inspection reveals that this is indeed true in the case of bubble-free ice, where the Pearson cross-correlation coefficient between the minimum pixel value and the mean grey value is 0.96 (for the maximum resolution of one pixel). In contrast, the same correlation coefficient in the case of bubbly ice takes significantly lower values of 0.61 (for a resolution of one millimetre) and 0.68 (for the maximum resolution of one pixel). Therefore, it transpires that the minimum pixel value contains some information that is not readily available to the mean grey value, in the case of bubbly ice. What this extra information may tell us requires further investigation, which is beyond the scope of this work. We can only speculate that it could be related either to the light scattering of microinclusions or to a multiscattering effect of the air bubbles.

Finally, in Fig. 10 we show a collection of 5 cm long grey-value profiles from eight representative depths, together with their respective mean annual-layer thicknesses (λ), derived from the AICC2012 chronology (Veres et al., 2012). As demonstrated by previous studies (Svensson et al., 2005; Takata et al., 2004; Winstrup et al., 2012), on this mesoscale it is sometimes possible to identify annual layers for estimating past accumulation. It is therefore tempting to associate the distances between grey-value peaks in Fig. 10 with λ, but a reliable identification of such peaks would require a mesoscopic analysis of high-resolution climate records, which is beyond the scope of this work. Below 2416 m depth the stratigraphy is severely disrupted, and consequently, there is no estimate of λ for those deeper depths. Thus, the peaks observed in the 2563 m sample are deceptive and should not be confounded with seasonal peaks.

It should also be remarked that in a low-accumulation site such as the EPICA-DML ($\approx$ 65 kg $m^{-2}a^{-1}$; Oerter et al., 2009), there is always the risk of a discontinuous record of snow accumulation, even close to the surface, as persistent winds may repeatedly redistribute the deposited snow on a decametre scale

(Faria et al., 2009; Birnbaum et al., 2010). Therefore, support from independent data is needed in order to estimate gaps in the accumulation record.

4. CONCLUSIONS

In this work we investigated the optical stratigraphy of the EPICA-DML (European Project for Ice Coring in Antarctica, Dronning Maud Land) deep ice core, through the analysis of a continuous collection of high-resolution (115 px cm^{-1}) line-scan images covering the depth range 450–2774 m, called the EDML-LS images (Faria et al., 2018). After a preliminary image processing, we performed a macroscale (1–10^3 m) digital analysis of the EDML-LS images, characterized by the combination of two main measures: grey value (arithmetic mean of the grey value in a region of the image) and a novel proxy of air bubble concentration (binarized bright-spot concentration).

Similar to other deep ice cores from Antarctica, the EPICA-DML deep ice core is characterized by two main depth zones: a *bubbly-ice zone* (88–1200 m depth) and a *bubble-free ice zone* (1200–2774 m depth). Within the bubbly-ice zone, the EDML-LS images reveal an optical stratigraphy that is washed out by the intense brightness caused by the strong light scattering by air bubbles. Therefore, in order to study the optical stratigraphy of this zone, we have proposed here a new proxy for air bubble concentration, based on the analysis of binarized bright spots. Through this binarized bright-spot analysis we could establish that layering in this zone is dominated by variations in bubble concentration (mainly in number, and to a lesser extent also in size). Furthermore, the combination of bright-spot analysis with the EDML mineral-dust record (used here as a proxy for microinclusions in Antarctic ice) allowed us to extend to the macroscale (1–10^3 m) a previous finding from microscopic studies (Faria et al., 2010; Bendel et al., 2013; Ueltzhöffer et al., 2010) that the air bubble concentration correlates with the concentration of microinclusions. Finally, we could show that the binarized bright-spot analysis provides a simple and fast way to produce the depth profiles of mean bubble size and bubble number density, which were previously obtained through laborious and painstaking microscopic measurements by Ueltzhöffer et al. (2010) and Bendel et al. (2013).

As for the bubble-free-ice zone, we used the mean grey value of the EDML-LS images to extend to the macroscale the correlation between optical stratigraphy and mineral dust concentration, which was microscopically observed in previous studies of cloudy bands (Gow and Williamson, 1976; Kipfstuhl et al., 2006, Faria et al., 2010, 2014b). This is a new and important result, because it demonstrates that the optical stratigraphy of bubble-free ice does record the past climate quite reliably on the macroscale.

To sum up, our general conclusion is that there is still a great and unexplored potential in the multiscale digital analysis of line-scan images of ice cores. The key is to not rely on a single measure, but rather to combine multiple measures that highlight different aspects of the optical stratigraphy. For bubble-free ice, conventional grey-value measurements provide the best description of the optical stratigraphy. For bubbly ice, we recommend combining grey value (for a general description of the optical stratigraphy) with binarized bright-spot analysis, which together provide a quite reliable and detailed picture of the bubbly-ice stratigraphy, including depth profiles of mean bubble size and bubble number density, without the need to embark on laborious and time-consuming microscopic analyses.

Modern digital imaging of ice cores is a field that is still in its infancy. With every study we unravel the great potential of new techniques for digital image acquisition and analysis. In order to promote the development of this field, it is utterly important to provide open access to all images and techniques, so that the whole community may profit from these discoveries and be able to investigate the ice cores again and again —without the risk of melting the ice.

Acknowledgements

The authors are grateful to Anders Svensson and an anonymous reviewer for valuable comments and suggestions to the manuscript, as well as to Thijs van Kolfschoten and Alejandro Cearreta for the editorial work. SHF thanks also the whole glaciology section of AWI for hosting him at the EPICA-DML drilling site (Kohnen Station) to participate in the EDML 2003–2004 and 2005–2006 drilling campaigns. This work is a contribution to the European Project for Ice Coring in Antarctica (EPICA), a joint European Science Foundation/European Commission scientific programme, funded by the EU and by national contributions from Belgium, Denmark, France, Germany, Italy, the Netherlands, Norway, Sweden, Switzerland, and the United Kingdom. The main logistic support was provided by IPEV and PNRA (at Dome C) and AWI (at Dronning Maud Land). This is EPICA publication no. 314. This research is supported by the Spanish Government through the María de Maeztu excellence accreditation 2018–2022 (Ref. MDM-2017-0714), and by the Basque Government through the BERC 2018–2021 programme. SHF acknowledges support from the Spanish Ministry of Science, Innovation, and Universities (MCIU) through the project iMechPro (RTI2018–100696–B–I00), and from the Ramón y Cajal grant RYC–2012–12167 of the Spanish Ministry of Economy, Industry and Competitiveness (MINECO).

Author contributions statement

All authors: resources, data curation, and writing—review and editing. *GMJ and SHF:* conceptualization, methodology, validation, investigation, visualization, and writing—original draft. *GMJ:* Software, formal analysis. *SHF:* supervision, project administration and funding acquisition.

REFERENCES

Bendel,V., Ueltzhöffer,K. Freitag,J, Kipfstuhl,S, Kuhs,W. Garbe,C. Faria, S.H. 2013. High-resolution variations in size, number and arrangement of air bubbles in the EPICA DML (Antarctica) ice core; Journal of Glaciology, Vol. 59, No. 217, 972–980. doi: 10.3189/2013JoG12J24.

Birnbaum, G., Freitag, J., Brauner, R., König-Langlo, G., Schulz, E., Kipfstuhl, S., Oerter, H., Reijmer, C., Schlosser, E., Faria, S.H., Ries,H., Loose, B., Herber, A., Duda, M.,. Powers, J., Manning, K., Van den Broeke, M. 2010. Strong-wind events and their influence on the formation of snow dunes: observations from Kohnen station, Dronning Maud Land, Antarctica; Journal of Glaciology, Vol. 56, No. 199, 891–902.

Dome Fuji Ice Core Project Members, 2017. State dependence of climatic instability over the past 720,000 years from Antarctic ice cores and climate modeling. Science Advances 3 (2), e1600446 DOI: 10.1126/sciadv.1600446.

Eichler, J., Weikusat, C., Wegner, A., Twarloh, B., Behrens, M., Fischer, H., Hörhold, M., Jansen, D., Kipfstuhl, S., Ruth, U., Wilhelms, F., Weikusat, I. (2019) Impurity analysis and microstructure along the climatic transition from MIS 6 into 5e in the EDML ice core using cryo-Raman microscopy. Frontiers in Earth Science 7, a20. doi: 10.3389/feart.2019.00020.

EPICA Community Members, 2006. One-to-one coupling of glacial climate variability in Greenland and Antarctica. Nature 444 (7116), 195–197.

EPICA Community Members, 2004. Eight glacial cycles from an Antarctic ice core. Nature 429 (6992), 623–628.

Faria, S.H.; Freitag, J.; Kipfstuhl, S. 2010. Polar ice structure and the integrity of ice-core paleoclimate records. Quaternary Science Reviews 29, 338–351.

Faria, S. H., Kipfstuhl, S., Azuma, N., Freitag, J., Hamann, I., Murshed, M. M., et al. 2009. The multiscale structure of Antarctica. Part I: inland ice. Low Temperature Science, 68, 39–59.

Faria, S. H.; Kipfstuhl, S.; Lambrecht, A. 2018. The EPICA-DML Deep Ice Core. A Visual Stratigraphy Record. Springer: Heidelberg.

Faria, S. H., Weikusat, I., Azuma, N. 2014a. The microstructure of polar ice. Part I: highlights from ice core research. Journal of Structural Geology, 61, 2–20.

Faria, S. H., Weikusat, I., Azuma, N. 2014b. The microstructure of polar ice. Part II: state of the art. Journal of Structural Geology, 61, 21–49.

Fischer, H., Fundel, F., Ruth, U., Twarloh, B., Wegner, A., Udisti, R. et al. 2007. Reconstruction of millennial changes in dust emission, transport and regional sea ice coverage using the deep EPICA ice cores from the Atlantic and Indian Ocean sector of Antarctica. Earth and Planetary Science Letters, 260(1–2), 340–354.

Gow, A.J., Meese, D.A., Alley, R.B., Fitzpatrick, J.J., Anandakrishnan, S., Woods, G.A., Elder, B.C., 1997. Physical and structural properties of the Greenland ice sheet project 2 ice core: a review. Journal of Geophysical Research 102, 26559–26575.

Gow, A.J., Williamson, T., 1976. Rheological implications of the internal structure and crystal fabrics of the West Antarctic ice sheet as revealed by deep core drilling at Byrd Station. Geol. Soc. Am. Bull. 87, 1665–1677.

Hammer, Ø., Harper, D.A.T., Ryan, P.D., 2001. PAST: Paleontological statistics software package for education and data analysis. Palaeontologia Electronica 4(1), Article 4.

Hecht, E. 1987. Optics. 2nd Edn. Addison-Wesley, Reading.

Iizuka, Y., Miyake, T., Hirabayashi, M., Suzuki, T., Matoba, S., Motoyama, H., Fujii, Y., Hondoh, T. 2009. Constituent elements of insoluble and non-volatile particles during the Last Glacial Maximum exhibited in the Dome Fuji (Antarctica) ice core. Journal of Glaciology 55(191), 552–562. DOI: 10.3189/002214309788816696.

Kawamura, K., Parrenin, F., Lisiecki, L., Uemura, R., Vimeux, F., Severinghaus, J.P., Hutterli, M.A., Nakazawa, T., Aoki, S., Jouzel, J., Raymo, M.E., Matsumoto, K., Nakata, H., Motoyama, H., Fujita, S., Goto-Azuma, K., Fujii, Y., Watanabe, O., 2007. Northern hemisphere forcing of climatic cycles in Antarctica over the past 360000 years. Nature 448, 912–916.

Kipfstuhl, S., Hamann, I., Lambrecht, A., Freitag, J., Faria, S.H., Grigoriev, D., Azuma, N., 2006. Microstructure mapping: a new method for imaging deformation-induced microstructural features of ice on the grain scale. J. Glaciol. 52 (178), 398–406.

Lambrecht, A., Kipfstuhl, J., Wilhelms, F., and Miller, H. 2004. Visual stratigraphy of the EDML ice core with a linescanner. Alfred Wegener Institute, Helmholtz Centre for Polar and Marine Research, Bremerhaven, PANGAEA, http://doi.pangaea.de/10.1594/PANGAEA.208005 (unpublished dataset).

McGwire, K., McConnell, J., Alley, R., Banta, J., Hargreaves, G, Taylor, K. 2008. Instruments and Methods Dating annual layers of a shallow Antarctic ice core with an optical scanner; Journal of Glaciology, Vol. 54, No. 188, 831–838.

Mie, G. 1908. Considerations on the optics of turbid media, especially colloidal solutions. Annalen der Physik. Nº 4. Vol. 25, 377–445.

NorthGRIP Members, 2004. High-resolution record of the Northern Hemisphere climate extending into the last interglacial period. Nature 431, 147–151.

Oerter H, Drücker, C; Kipfstuhl, S. Wilhelms, F. 2009. Kohnen Station – the Drilling Camp for the EPICA Deep Ice Core in Dronning Maud Land; Polarforschung 78 (1-2), 1–23.

Ohno, H., Igarashi, M., Hondoh, T. 2006. Characteristics of salt inclusions in polar ice from Dome Fuji, East Antarctica. Geophysical Research Letters 33, L08501/1–5.

Oyabu, I., Iizuka, Y., Kawamura, K., Wolff, E., Severi, M., Ohgaito, R., Abe-Ouchi, A., Hansson, M. 2020. Compositions of dust and sea salts in the Dome C and Dome Fuji ice cores from Last Glacial Maximum to early Holocene based on ice-sublimation and single-particle measurements. Journal of Geophysical Research: Atmospheres 125, e2019JD032208. DOI: 10.1029/2019JD032208.

Rey D., Neuhäuser M. 2011. Wilcoxon-Signed-Rank Test. In: Lovric M. (eds) International Encyclopedia of Statistical Science. Springer, Berlin, Heidelberg

Ridler, T.W., Calvard, S. 1978. Picture thresholding using an iterative selection method. IEEE Transactions on Systems, Man and Cybernetics 8, 630–632.

Schneider, C.A.; Rasband, W.S., Eliceiri, K.W. 2012. NIH Image to ImageJ: 25 years of image analysis. Nature methods 9(7): 671–675.

Sakurai, T., Ohno, H., Horikawa, S., Iizuka, Y., Uchida, T., Hondoh, T. 2010. A technique for measuring microparticles in polar ice using micro-Raman spectroscopy. International Journal of Spectroscopy 2010, 384956. DOI:10.1155/2010/384956.

Schulz, M., Mudelsee, M. 2002. REDFIT: estimating red-noise spectra directly from unevenly spaced paleoclimatic time series. Computers & Geosciences 28, 421–426.

Svensson, A., S. W. Nielsen, S. Kipfstuhl, S. J. Johnsen, J. P. Steffensen, M. Bigler, U. Ruth, R. Röthlisberger. 2005. Visual stratigraphy of the North Greenland Ice Core Project (NorthGRIP) ice core during the last glacial period, J. Geophys. Res., 110, D02108, doi: 10.1029/2004JD005134.

Takata, M., Iizuka,Y., Hondoh,T., Fujita,S., Fujii,Y., Hitoshi Shoji, H. 2004.Stratigraphic analysis of Dome Fuji Antarctic ice core using an optical scanner. Annals of Glaciology 39, 467–472.

Ueltzhöffer,K., Bendel,V., Freitag, J., Kipfstuhl, S., Wagenbach, D., Faria, S.H., Garbe, C.S. 2010. Distribution of air bubbles in the EDML and EDC (Antarctica) ice cores, using a new method of automatic image analysis; Journal of Glaciology, Vol. 56, No. 196, 339–348.

Veres, D., Bazin, L., Landais, A., Toyé Mahamadou Kele, H., Lemieux-Dudon, B., Parrenin, F., Martinerie, P., Blayo, E., Blunier, T., Capron, E., Chappellaz, J., Rasmussen, S. O., Severi, M., Svensson, A., Vinther, B., Wolff, E. W. 2013. The Antarctic ice core chronology (AICC2012): An optimized multi-parameter and multi-site dating approach for the last 120 thousand years, Climate of the Past. 9, 1733-1748. DOI:10.5194/cp-9-1733-2013.

Wegner, A., Fischer, H. Delmonte, B. Petit, J.-R. Erhardt, T. Ruth, U. Svensson, A. Vinther, B. Miller,H. (2015); The role of seasonality of mineral dust concentration and size on glacial/interglacial dust changes in the EPICA Dronning Maud Land ice core; J. Geophys. Res. Atmos., 120, 9916–9931, doi:10.1002/2015JD023608.

Winstrup, M. 2011. An Automated Method for Annual Layer Counting in Ice Cores and an application to visual stratigraphy data from the NGRIP ice core. PhD Thesis. Faculty of Science University of Copenhagen.

Winstrup, M, Svensson, A, Rasmussen, S, Winther, O., Steig, E., Axelrod, A. 2012. An automated approach for annual layer counting in ice cores; Clim. Past, 8, 1881–1895.

Wolff, E.W., H. Fischer, F. Fundel, U. Ruth, B. Twarloh, G. C. Littot, R. Mulvaney, R. Röthlisberger, M. de Angelis, C. F. Boutron, M. Hansson, U. Jonsell, M. A. Hutterli, F. Lambert, P. Kaufmann, B. Stauffer, T. F. Stocker, J. P. Steffensen, M. Bigler, M. L. Siggaard-Andersen, R. Udisti, S. Becagli, E. Castellano, M. Severi, D. Wagenbach, C. Barbante, P. Gabrielli, V. Gaspari, 2006. Southern Ocean sea-ice extent, productivity and iron flux over the past eight glacial cycles. Nature 440, 491–496. DOI:10.1038/nature04614.

Zúñiga, I; Crespo, E. 2010. Unidades Didácticas; Meteorología y Climatología/Universidad Nacional de Educación a Distancia, Madrid. 30-33. ISBN: 978-84-362-6082-3

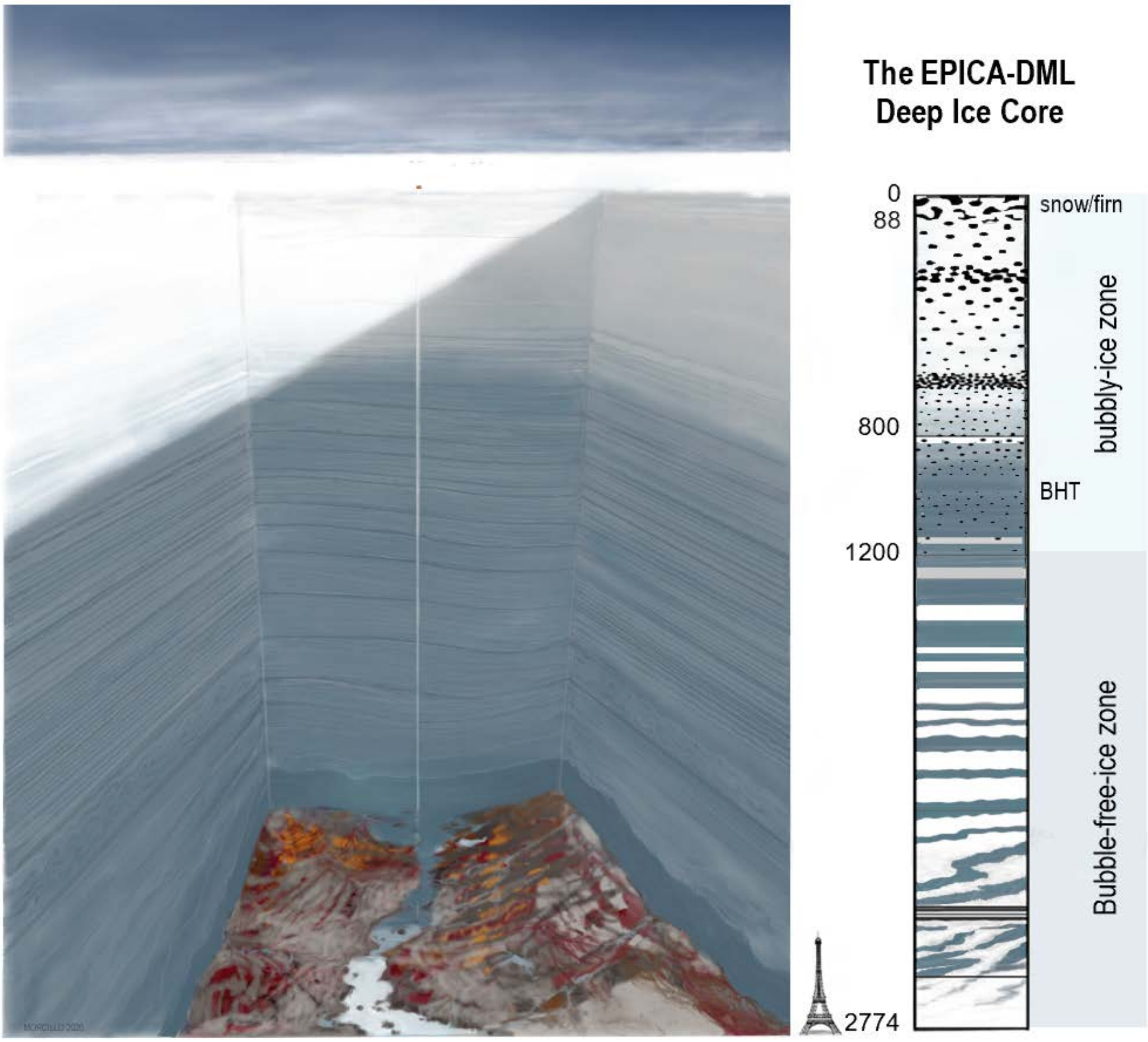

Figure 1. Artistic interpretation of a cross-sectional view of the EPICA-DML deep-drilling site (75°00’09”S, 00°04’06”E). Main stratigraphic features of snow, firn, bubbly ice, and bubble-free ice are illustrated in the schematic representation of the EPICA-DML deep ice core on the right. The numbers represent depth in metres and BHT stands for Bubble–Hydrate Transition zone (see text for more details). For comparison, a drawing of the Eiffel Tower is presented on scale, at the base of the figure. North is to the right of the illustration. The ice flows westwards along the valley, that is, from the observer into the plane of the figure. The illustration was created by G. Morcillo Juliani, with the ice-core summary on the right side adapted from Faria et al. (2010, 2018).

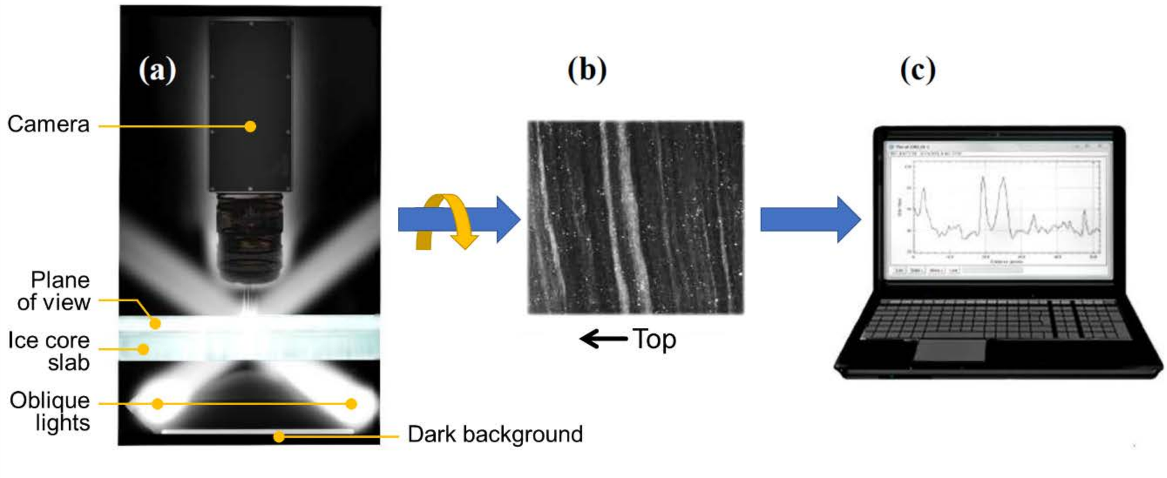

Figure 2. Line-scan device scheme. The camera (a) moves synchronously with the dark field illumination system (oblique lights), travelling the entire ice-core slab while capturing the image of a thin line one-pixel wide at each step. This generates a high-resolution (115 px cm^{-1}) digital image without optical deformations in 8-bit greyscale format (b), which can finally be processed by a computer (c). Notice that, in the passage from (a) to (b), the "plane of view" indicated in (a) undergoes a 90° rotation about the long axis of the core in order to show the image (b) on the plane of the page. The graphic shown in (c) is the grey-value record of the image (b). In all three panels, top of the core is to the left.

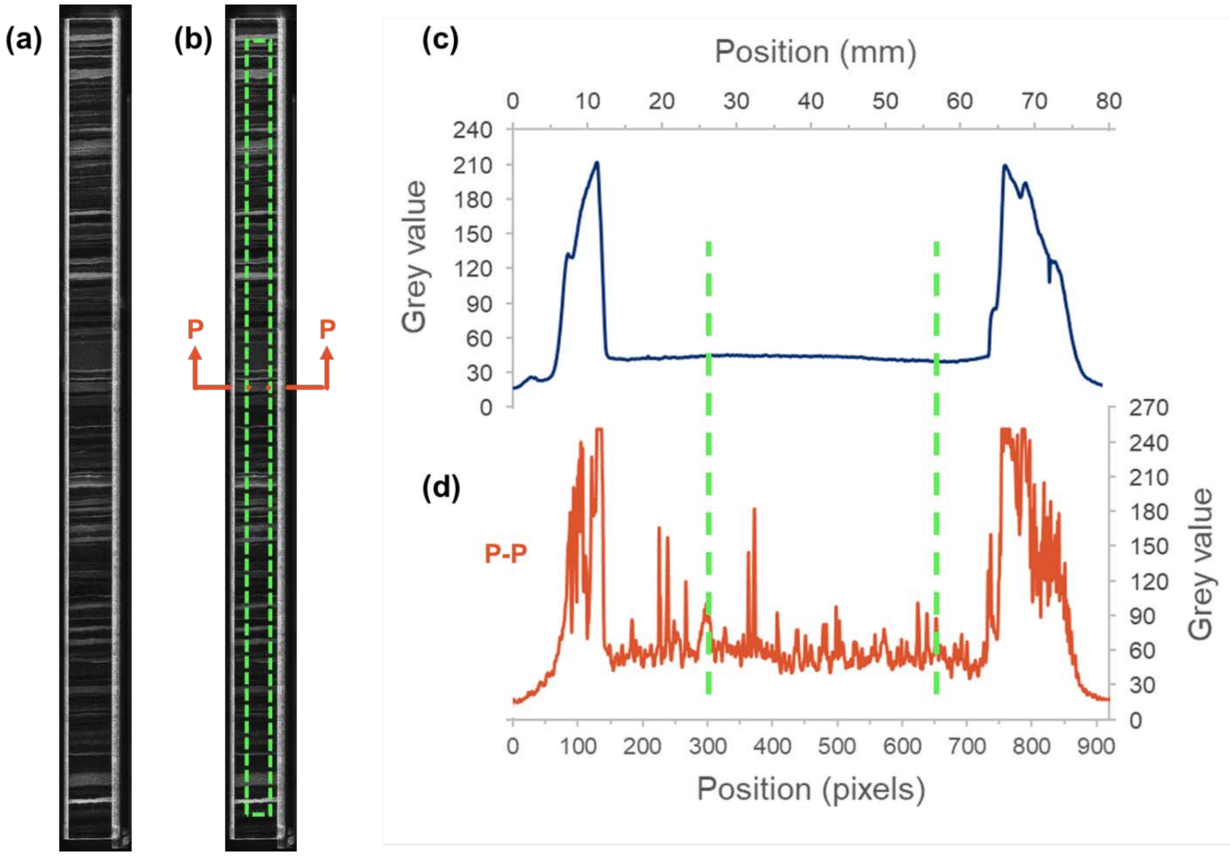

Figure 3. Example of selected region for macroscopic analysis. (a) One-metre slab of the EDML deep ice core from 1802 m depth. Cloudy bands are clearly visible because this is bubble-free ice. (b) Same LS image with the region selected for the macroscopic analysis (dashed-green rectangle). For instance, the mean grey value of the whole ice-core slab is the arithmetic mean of the grey values of all pixels within the dashed-green region. (c) Cross-sectional view of grey values averaged over the whole length of the ice slab. (d) Cross-sectional view of grey values along a single line of pixels, indicated by the dash-dotted-red line P-P. The selected region for microscopic analysis, denoted by the dashed-green rectangle in (b), is also indicated in (c) and (d), showing that effects from the border of the core are excluded from the analysis.

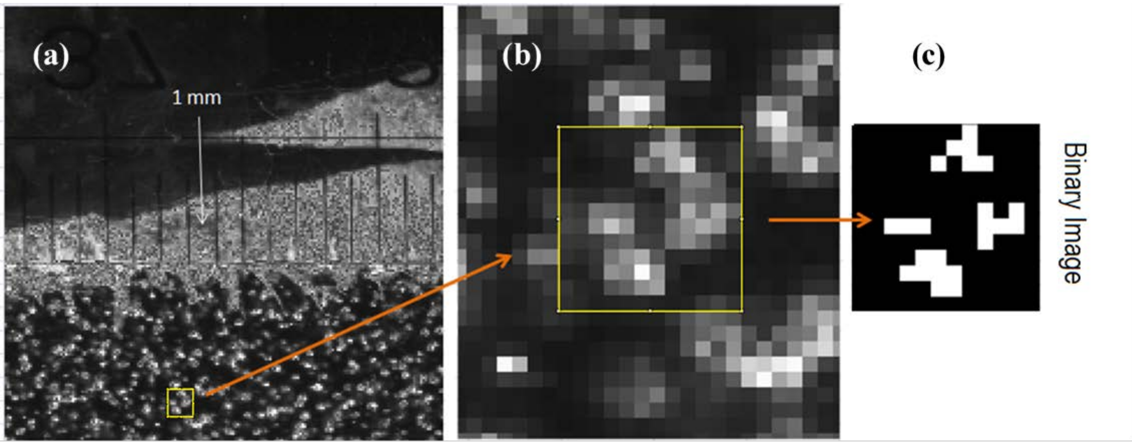

Figure 4. Binarization process. (a): Part of the original 8-bit greyscale EDML LS image. (b): Zoom into a 1 mm^2 region inside the image (yellow square), showing four bubbles (bright spots). (c): Result of the binarization process within the yellow square.

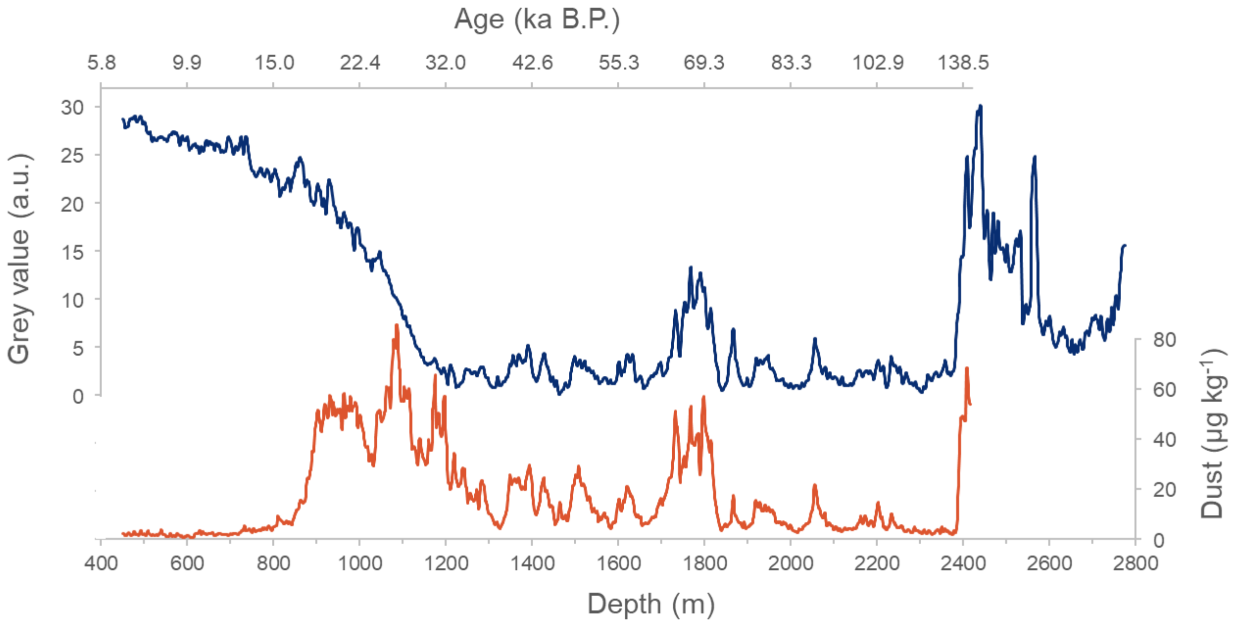

Figure 5. EPICA-DML deep ice core profiles of mean grey value (dark blue, above) and mineral dust (red, below). The correlation between dust concentration and grey value is evident through most of the core. Conspicuous is also the correlation loss in the upper depth range, from 450 to 1200 m, which corresponds to the bubbly-ice zone. High grey values observed in that zone are caused by the intense light scattering by air bubbles, which turns the line-scan images of bubbly ice bright. The age scale on the top is obtained from the AICC2012 chronology (Veres et al., 2012). For better visualization, both records have been slightly smoothened with the LOWESS algorithm of the software PAST (Hammer et al., 2001) with a quite small smoothing parameter of 0.004.

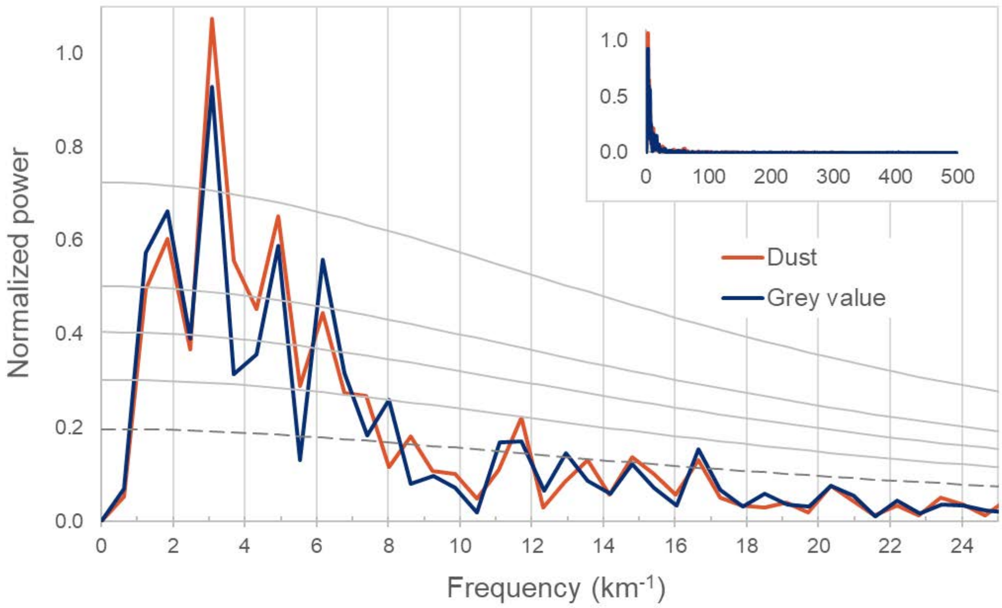

Figure 6. Comparison of the power spectra of mean grey value and dust concentration displayed in Fig. 5 within the depth range of bubble-free ice (1200–2416 m). The dashed grey curve describes the red-noise level derived from the first-order autoregressive model AR(1). The solid grey curves are significance lines of (from bottom) 80 %, 90 %, 95 %, and 99 % chi-squared bounds for an AR(1) hypothesis. The small insert on top right shows the complete power spectra up to the Nyquist frequency (500 km^{-1}). Correlation is generally very good, especially for the frequencies above the red-noise level (except for a minor mismatch around 8 km^{-1}, discussed in the text). All data were calculated with the software PAST (Hammer et al., 2001) using the REDFIT procedure (Schulz and Mudelsee, 2002).

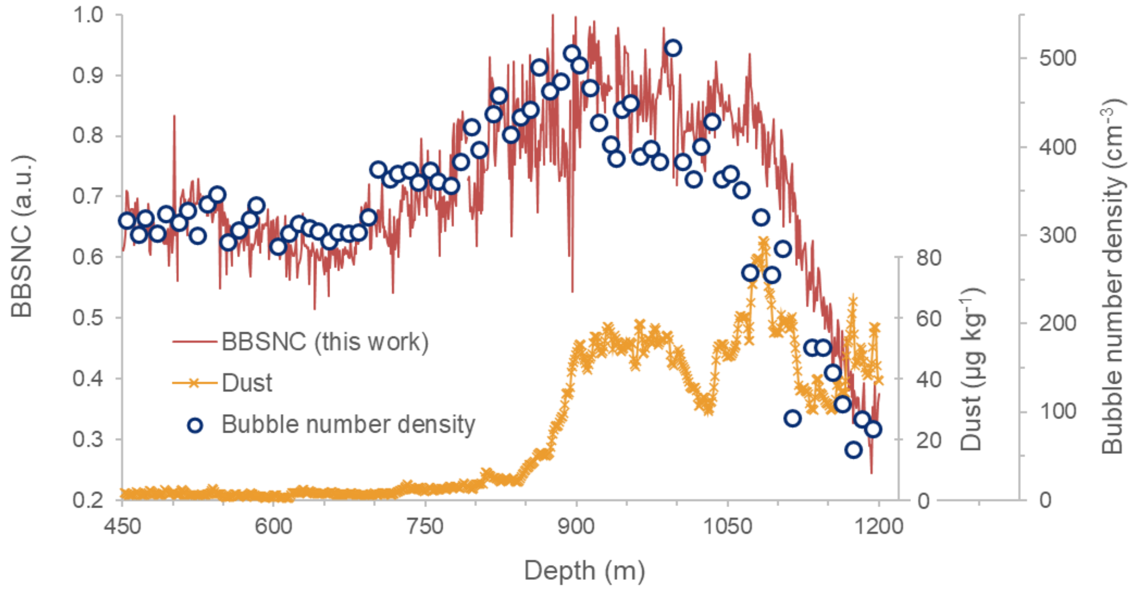

Figure 7. Comparison of the proxy for bubble number density proposed in this work (binarized-bright-spot normalized counting, BBSNC) with dust data (Fischer et al., 2007) and the rigorous microscopic measurements of bubble number density by Bendel et al. (2013), for the whole bubbly-ice zone where the data coexist (450-1200 m depth). Dust data has been slightly smoothened as described in Fig. 5.

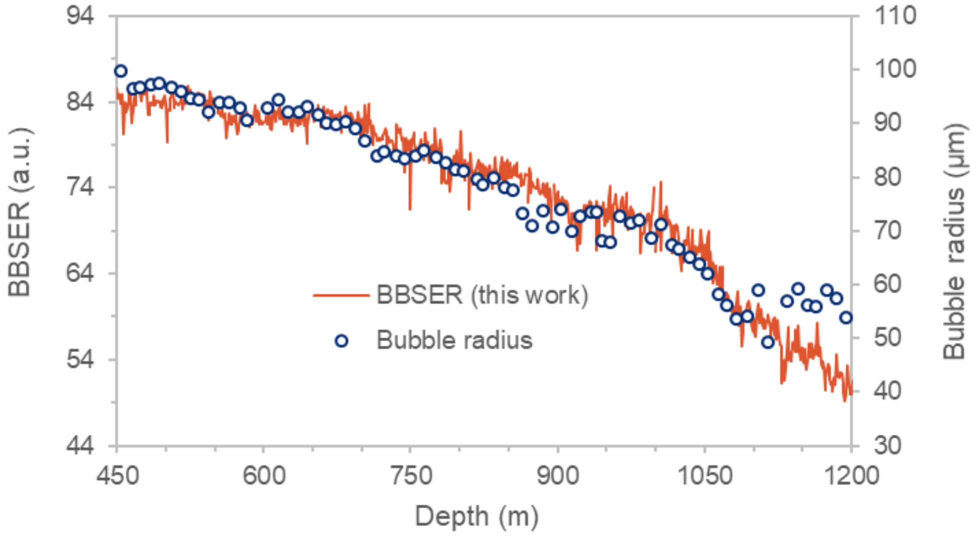

Figure 8. Comparison of the proxy for average bubble size proposed in this work (binarized-bright-spot equivalent radius, BBSER, which is proportional to the square root of the binarized-bright-spot area) with the rigorous microscopic measurements of average bubble size by Bendel et al. (2013), for the whole bubbly-ice zone where the data coexist (450–1200 m depth).

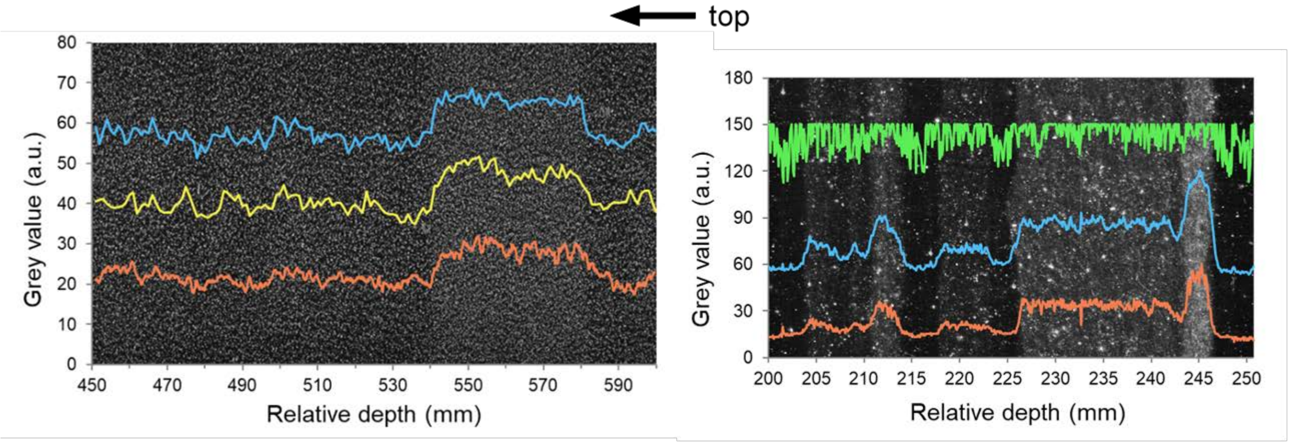

Figure 9. Mesoscopic details of two LS images of the EPICA-DML deep ice core. *Left:* bubbly-ice sample from 449.45–449.60 m depth (annual layer thickness, λ = 56 mm, Veres et al., 2013). The bright spots are produced by the light scattered by bubbles and serve as a proxy for bubble concentration. Three profiles are superposed on the image: mean grey value (blue, top), bubble-counting proxy (binarized bright-spot counting, yellow, middle) and minimum pixel value (red, bottom). *Right:* bubble-free ice sample from 1366.20–1366.25 m depth (λ = 19 mm). The glittering spots are caused by specular reflections within the ice, possibly related to relaxation features (a topic for future research). Cloudy bands are clearly discernible. The superposed profiles are maximum pixel size (green, top), mean grey value (blue, middle), and minimum pixel value (red, bottom). Notice the different horizontal scales of the two figures: 150 mm on the left and 50 mm on the right. The profiles on the left have a resolution of 1 mm, while the profiles on the right have full resolution (1 pixel). See the text for more details.

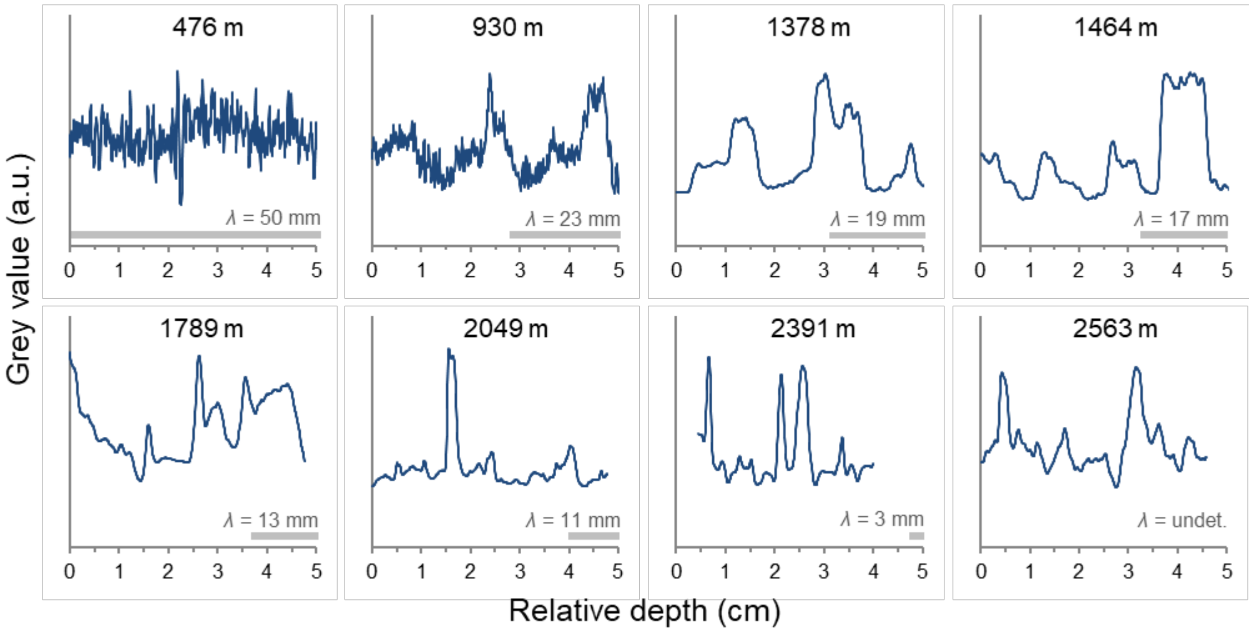

Figure 10. Grey-value profiles (5 cm long each) from eight representative depths of the EPICA-DML deep ice core. To enhance visibility, each graph has its own optimized range of grey values, in arbitrary units. The annual-layer thickness (λ) is estimate from the AICC2012 chronology (Veres et al., 2012). Below 2416 m depth the stratigraphy is disrupted and consequently λ is undetermined for the sample from 2563 m depth. The effect of bubbles on the grey intensities in the bubbly-ice zone (88–1200 m depth) is evident. Conspicuous is also the regularity of cloudy bands in the upper part of the bubble-free-ice zone (1200–1700 m depth, called "MIS3 zone" by Faria et al., 2018), where cloudy bands are still flat and undisturbed by the ice flow, as well as comparatively thick.